

Research paper

S-nitrosogluthathione reductase activity of amphioxus ADH3: insights into the nitric oxide metabolism

Laura Godoy, Roser González-Duarte and Ricard Albalat

Departament de Genètica. Facultat de Biologia. Universitat de Barcelona. 08028 Barcelona, Spain.

Corresponding address: Ricard Albalat, Departament de Genètica, Facultat de Biologia, Universitat de Barcelona. Av. Diagonal, 645. 08028 Barcelona, Spain. Tel.: +34.934029009; Fax: +34.934034420; E-mail: ralbalat@ub.edu

Received: 2006.02.06; Accepted: 2006.04.09; Published: 2006.05.05

Nitric oxide (NO) is a signalling molecule involved in many physiological functions. An important via of NO action is through the S-nitrosylation of proteins, a post-translational modification that regulates the activity of enzymes, protein-protein interactions and signal transduction pathways. Alcohol dehydrogenase class III (ADH3) recognises S-nitrosoglutathione (GSNO), the main reservoir of non-protein S-nitrosothiol, and functions as an effective GSNO reductase (GSNOR) and as a safeguard against nitrosative stress. To investigate the evolutionary conservation of this metabolic role, we have produced recombinant *Branchiostoma floridae* ADH3. Pure preparations of ADH3 showed 2-fold higher activity as GSNOR than as formaldehyde dehydrogenase, the previously assumed main role for ADH3. To correlate ADH3 expression in the gut with areas of NO production, we analysed the tissue distribution of the nitric oxide synthase (NOS) enzyme in amphioxus larvae. Immunostaining of the NOS enzyme revealed expression in the gut and in the dorsal region of the club-shaped gland. Co-localization in the gut supports the ADH3 and NOS joint contribution to the NO/SNO homeostasis.

Key words: Cephalochordate, alcohol dehydrogenase class III (ADH3), nitric oxide synthase (NOS), intestine, club-shaped gland.

1. Introduction

Nitric oxide (NO) is a diffusible highly reactive gas produced by the enzymatic conversion of L-arginine by nitric oxide synthases (NOS). NO possesses an unusually large repertory of physiological functions and it is probably one of the oldest bioregulatory systems controlling metazoan physiology [1]. In addition to the well-documented roles of NO in vertebrates (reviewed in [2]), many studies also support the functional relevance of NO in invertebrates [3-8]. Classically, NO action had been associated with the cGMP signalling pathway. However, the current picture points to additional mechanisms for NO bioactivity such as S-nitrosylation of cysteine thiols (SNO) [2, 9], a post-translational protein modification that regulates the activity of metabolic enzymes, structural proteins or transcription factors [10]. Although specific enzymatic mechanisms involved in protein S-nitrosylation have not yet been described, degradation of S-nitrosoglutathione (GSNO) promotes the denitrosylated state and so, GSNO turnover, significantly influences the level of whole-cell S-nitrosylation.

GSNO is mainly degraded by an NADH-dependent S-nitrosoglutathione reductase (GSNOR) activity [11], associated to the medium-chain alcohol dehydrogenase class III (MDR-ADH3) enzyme, also known as glutathione-dependent formaldehyde dehydrogenase (FALDH) [11-14]. ADH3 enzymes had

been involved in formaldehyde metabolism, oxidising S-hydroxymethylglutathione (HMGSH) to S-formylglutathione [15]. However, the high specificity of ADH3 towards GSNO [12] and the fact that yeast and mouse ADH3 knockouts devoid of GSNOR activity show a substantial increase of S-nitrosylated proteins [9, 11] have established a direct relation of ADH3 with NO metabolism.

ADH3 enzymes have been identified in most major life forms, ranging from bacteria to animals. ADH3 is the only member of the MDR-ADH family found in non-vertebrate organisms, and is considered the archetypal form from which multiple gene duplications expanded the vertebrate ADH family into at least eight different classes (ADH1-8) (reviewed in [16]). In previous studies, we showed that in contrast to the widespread expression pattern of the vertebrate *Adh3*, the expression of the *Adh3* in non-vertebrate organisms (e.g. arthropods, ascidians and cephalochordates) is restricted to the digestive system [17, 18]. This finding suggested that the ADH family expansion during early vertebrate evolution was accompanied by a change in the *Adh3* expression pattern, and challenged the role that had been classically attributed to ADH3 as a housekeeping enzyme in charge of formaldehyde elimination [18]. In this work, we provide the first evidence that ADH3 might be involved in NO homeostasis in the cephalochordate *Branchiostoma floridae*. Pure preparations of recombinant amphioxus ADH3 showed *in vitro* the ability to reduce GSNO, indeed a

better substrate than HMGSH, the intermediate product in formaldehyde metabolism. Moreover, to correlate ADH3 expression with NO production, we have performed immunostaining of NOS in developing larvae, and showed ADH3/NOS co-localization in mid- and hind-gut areas.

2. Materials and Methods

Electrophoresis and enzymatic activity staining of crude extracts

To detect GSNO reductase and formaldehyde dehydrogenase activities, six amphioxus adults were homogenized in 2 ml of degassed 0.1 M sodium pyrophosphate, 0.1 mM DTT, and centrifuged at 20,000 g for 20 min. Protein concentration of the crude extracts was determined colorimetrically. Enzymatic activity was assessed after electrophoresis on non-denaturing 7.5% polyacrylamide gel. For formaldehyde dehydrogenase activity, gels were incubated in 0.1 M sodium pyrophosphate pH 8.0, 0.5 M KCl, 1 mM reduced glutathione and 5 mM formaldehyde at 37 °C [19]. After 5 minutes, nitroblue tetrazolium and phenazine methosulfate were added at a final concentration of 0.1 mM each. For GSNO reductase activity, gels were incubated in 0.1 M sodium pyrophosphate at pH 7.4 with 2 mM NADH, for 15 min in an ice-bath [14]. Excess buffer was drained and gels were covered with filter paper strips soaked in GSNO. After 15 min, the filter paper was removed and the gel was exposed under ultraviolet light to observe the disappearance of the NADH fluorescence.

Expression and purification of recombinant *B. floridae* ADH3

The full-length coding region of *B. floridae* *Adh3* cDNA [17] was PCR amplified with the sense primer 5'-**TGGATCC**ATGGCGGACACTG-3', which introduces a *Bam*H I restriction site (underlined) next to the ATG (in bold), and the antisense primer 5'-**CGAATTCT**CAGAACGTGGATCAC-3', which places a *Eco*R I site (underlined) at the 3'-end. The PCR conditions were as follows: an initial denaturation step at 94°C for 5 min, followed by 40 cycles at 94°C for 45 s, 42°C for 1 min and 72°C for 2 min and a final extension step at 72°C for 5 min. The purified fragment was digested with *Bam*H I and *Eco*R I enzymes and cloned into the expression vector pRSETA (Invitrogen), to fuse a polyhistidine tag at the N-terminal of ADH3. The expression of His-ADH3 protein in *E. coli* BL21 (DE3) pLys was induced with 0.1 mM isopropyl-β-D-thiogalactopyranoside for 3 h at 37°C. Cells were harvested and disrupted by sonication in cold PBS. Protein extracts were collected after centrifugation at 20,000 g for 20 min at 4°C and His-ADH3 was partially purified with a Talon Metal Affinity Resin following the supplier's instructions (BD Biosciences Clontech, USA). Protein recovered after overnight treatment with enterokinase (EKMaxTM Enterokinase; Invitrogen) at 16°C, was loaded in Superdex200 FPLC column equilibrated

with 20 mM TrisHCl pH 8.0. Formaldehyde/GSH activity was tested in the collected fractions. From 500 ml culture, 5 µg of pure ADH3 was obtained with a specific activity with formaldehyde of 4.3 U/mg. Protein concentration was determined colorimetrically and purity was analysed by SDS-PAGE with Coomassie brilliant blue staining. Enzymatic activity of the purified recombinant protein was assayed *in situ* after electrophoresis as described in the previous section.

Kinetic studies

Formaldehyde dehydrogenase and GSNO reductase activities were tested at 25°C by monitoring the production of NADH at 340 nm ($\epsilon_{340} = 6,22 \text{ mM}^{-1} \text{ cm}^{-1}$) for formaldehyde oxidation or the consumption of NADH and GSNO ($\epsilon_{340} = 7,06 \text{ mM}^{-1} \text{ cm}^{-1}$) for GSNO reduction. The formaldehyde dehydrogenase activity was measured at pH 8.0 in 0.1 M sodium pyrophosphate, with S-hydroxymethylglutathione (HMGSH; formed by mixing formaldehyde and glutathione) and NAD⁺. GSNO reductase activity was measured at pH 7.5 in 0.1 M sodium pyrophosphate, with freshly prepared GSNO and NADH. Kinetic constants for NAD⁺ and NADH were determined with 1 mM of glutathione - 1 mM of formaldehyde, and with 0.3 mM of GSNO, respectively. Kinetic constants for HMGSH and GSNO were determined with 2.4 mM NAD⁺ and 0.3 mM NADH, respectively. Kinetic constants were calculated with the non-linear regression program Grafit (version 3.0, Eritacus Software), and expressed as the mean ± SD of at least three independent determinations. Catalytic constant (kcat) values were calculated using the protein molecular mass of 80,000 for the ADH3 dimer.

Amphioxus NOS and phylogenetic analysis

A *B. floridae* cDNA-NOS sequence was retrieved from GeneBank, accession number AF396968, and compared with available vertebrate and invertebrate sequences. The following NOS sequences were used in our study: AAK83069 (*Aplysia californica*, California sea hare), O61608 (*Anopheles stephensi*, mosquito), BAB85836 (*Bombix mori*, silk worm), CAB60197 (*Cyprinus carpio*, carp), XP_692103 and NP_571735 (*Danio rerio*, zebrafish), NP_523541 (*Drosophila melanogaster*, fruit fly), NP_990292 and XP_425296 (*Gallus gallus*, chicken), P29474, AAA36375 and P29475 (*Homo sapiens*, human), O61309 (*Lymnaea stagnalis*, great pond snail), O77104 (*Manduca sexta*, tobacco hornworm), P70313, AAM11887 and Q9Z0J4 (*Mus musculus*, mouse), CAC83069 (*Oncorhynchus mykiss*, rainbow trout), NP_068610, BAA07994 and P29476 (*Rattus norvergicus*, rat), Q26240 (*Rhodnius prolixus*, insect), XP_781703 (*Strongylocentrotus purpuratus*, sea urchin), AAM46138 (*Takifugu poecilonotus*). Frog sequences were taken from *Xenopus tropicalis* genome assembly 3.0 (JGI): fgenesh1_pg.C_scaffold_2000005, estExt_fgenesh1_pg.C_12630001 and fgenesh1_pg.C_scaffold_456000016. Sequences were retrieved and corrected to maximize the similarity with known NOS enzymes.

Protein sequence alignments and a neighbour-joining (NJ) tree were generated with clustalX [20] and drawn with the TreeViewPPC program [21]. Confidence in each node was assessed by 1000 bootstrap replicates. Maximum likelihood (ML) analysis was performed using the quartet sampling and NJ parameter estimation procedure of TREEPUZZLE. The N-terminal region of the NOS isoforms (neuronal, inducible and endothelial) are highly variable in length and sequence, and produced unreliable alignments. This region was, therefore, excluded from the phylogenetic analyses and only alignments starting at the oxygenase domain (D352 of human nNOS) were considered.

Western blot and whole-mount immunostaining

For western blot, four *B. floridae* specimens were homogenized in cold PBS, 0.1 mM DTT and centrifuged at 20,000 g for 20 min. 0.5–1.0 mg of soluble protein was resolved on an SDS-PAGE and transferred into a polyvinylidene difluoride (PVDF) membrane. After 1 h in blocking buffer (10% fat-free milk in PBS), the membrane was incubated for 1 h with a universal anti-NOS antibody (anti-uNOS, Affinity Bioreagents Inc.), at 1:1000 dilution in 0.5% fat-free milk in PBS with 0.05% Tween-20. The anti-uNOS antibody is an affinity purified rabbit anti-NOS directed against a C-terminal epitope (DQKRYHEDIFG) that is highly conserved among the different NOS isoforms in vertebrates, insects and crustaceans [22]. Immunoreactive proteins were visualized by ECL Western blotting analysis system (Amersham Biosciences) after incubation for 1 h with peroxidase-conjugated goat anti-rabbit secondary antibody used at 1:2000 dilution.

B. floridae larvae were collected, fixed, and stored at -20°C in 70% ethanol. Immunostaining was performed as described [23] with minor modifications. Briefly, larvae were incubated in 1 ml ethanol/DMSO (1:1) for 3 min in ice, followed by 15 min at RT after addition of 250 µl Triton X-100. Larvae were rinsed 6 times, 10 min each, in TST (20 mM TrisHCl pH 7.4, 100 mM NaCl and 0.1% Triton X-100) and blocked for 30 min in TSTM (TST containing 5% fat-free milk). The larvae were incubated for 48 h at 4°C in rabbit anti-uNOS (Affinity Bioreagents Inc.) (dilution 1:100 in TSTM). After rinsed 7 x 20 min, the secondary antibody, donkey anti-rabbit IgG labeled with Rhodamine-red (Jackson Immunoresearch), was added (dilution 1:200) for 48 h at 4°C, and larvae were rinsed again 7 x 20 min. Finally, the samples were mounted using SlowFade light Antifade Kit (Molecular Probes) and observed by confocal microscopy (Leica TCS 4D).

3. Results

GSNO reductase activity of amphioxus ADH3

GSNO reductase activity was assessed spectrophotometrically in amphioxus homogenates, 4.2×10^{-3} U/mg. Non-denaturing gel electrophoresis of protein homogenates of whole adult animals

showed a very similar banding pattern for GSNO activity and formaldehyde/GSH staining (Figure 1, lanes 1 and 2), suggesting that both substrates are metabolised by the same enzyme. To further investigate this possibility, the cDNA of *B. floridae* Adh3 was expressed in *E. coli*. The recombinant protein was produced and purified to homogeneity (Figure 1, lanes 3, 4 and 5). In the pure preparation, the GSNO reductase and formaldehyde dehydrogenase activities were shown by native gel electrophoresis staining (Figure 1, lanes 6 and 7). The specific activities of the purified recombinant ADH3 were quantified by monitoring the absorbance at 340 nm with GSNO (65.6 U/mg) and HMGSH (4.3 U/mg) as substrates. The kinetic parameters of *B. floridae* ADH3 (Table 1) were examined under conditions allowing comparisons with those obtained for other class 3 forms. The Km value for the recombinant *B. floridae* ADH3 in front of HMGSH was essentially the same as that for the native *B. lanceolatum* ADH3 [17], but the kcat value (375 min^{-1}) was slightly lower than the one previously reported (680 min^{-1}). The catalytic efficiency of the recombinant *B. floridae* ADH3 for GSNO reduction was twice that of HMGSH oxidation, indicating the preference for GSNO reduction of the amphioxus enzyme. Yeast and human ADH3 enzymes are also active in HMGSH oxidation and GSNO reduction, with similar reductive vs. oxidative ratios than that for amphioxus enzyme: 2.3 and 1.9 times fold, respectively [14]. The comparison of human, amphioxus and yeast supports the reported constancy at the functional and structural level of class 3 enzymes [24, 25].

Figure 1. Amphioxus total protein homogenate (1.0 mg) resolved on non-denaturing 7.5% polyacrylamide gel electrophoresis and stained for formaldehyde dehydrogenase (lane 1) and GSNO reductase (lane 2) activities. Coomassie stained SDS/PAGE of samples corresponding to the different purification steps of recombinant *B. floridae* ADH3: 40 µg of total protein homogenate (soluble fraction) from an *E. coli* expressing *B. floridae* ADH3 (lane 3); 16 µg of partially purified ADH3 eluted from a Talon Metal Affinity Resin (BD Biosciences Clontech, USA) after enterokinase cleavage (lane 4), and 2.3 µg of pure recombinant enzyme after Superdex200 FPLC column (lane 5). Pure recombinant protein (2.0 µg) was loaded onto non-denaturing 7.5% polyacrylamide gel electrophoresis and stained for formaldehyde dehydrogenase (lane 6) and GSNO reductase (lane 7) activity

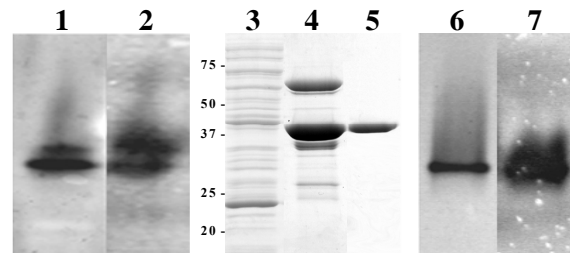


Table 1. GSNO and HMGSH activities of ADH3.

		<i>B. floridae</i> ^a	<i>B. lanceolatum</i>	<i>Drosophila</i>	Rat	Human	Human ^{1a}	Human ^{2a}	<i>S. cerevisiae</i> ^a
GSNO	Km (mM)	0.056 ± 0.009	-	-	0.028	-	0.027	0.027	0.15
	kcat (min ⁻¹)	10000 ± 520	-	-	2640	-	2400	12000	52600
	kcat/Km	178800 ± 25100	-	-	94300	-	90000	444400	350000
NADH	Km (mM)	0.045 ± 0.011	-	-	0.024	-	0.008	0.03	0.13
HMGSH	Km (mM)	0.004 ± 0.0006	0.0044	0.006	-	0.004	0.002	0.0014	0.02
	kcat (min ⁻¹)	375 ± 16	680	960	-	200	115	320	3100
	kcat/Km	87900 ± 9667	150000	160000	-	50000	58000	229000	155000
NAD	Km (mM)	0.008 ± 0.0018	0.011	0.13	-	0.009	0.007	0.007	0.045

Values are from this work (*B. floridae* ADH3) or from the literature (*B. lanceolatum*, *Drosophila* and Human ([17] and references therein); Rat [12]; Human¹ [26]; Human² and *S. cerevisiae* [14]). ^aThese values are from recombinant expressed enzymes.

Amphioxus nitric oxide synthase: phylogeny and immunodetection

To link the GSNOR activity of ADH3 with the production of NO/GSNO, we searched for amphioxus NOS sequences in databases and retrieved a *B. floridae* cDNA (AF396968) with clear homology with vertebrate *Nos* genes. This sequence matched to a unique *Nos* gene that was assembled from the available raw data of the amphioxus genome project. Comparison of the cDNA and the genomic sequences showed minor differences that were corrected to maximize the similarity with known NOS enzymes and allowed us to deduce the gene structure. The *B. floridae Nos* gene was made of 26 exons that expanded over 9.5 kb (data not shown), encoding a 1329 aa protein (Figure 2A) equally related with the three –iNOS, eNOS and nNOS– vertebrate forms. In accordance, in the phylogenetic tree, amphioxus NOS branched outside the clade comprising all vertebrate NOS (Figure 2B). This topology would be in agreement with a single *Nos* gene in an ancestral chordate.

NOS protein in adult amphioxus extracts was detected by western blot (Figure 3G) using an affinity purified rabbit anti-NOS antibody that specifically recognises a C-terminal epitope, DQKRYHEDIFG, highly conserved among NOS isoforms in vertebrates, insects and crustaceans [7, 22]. The deduced *B. floridae* sequence for this epitope is: DNNRYHEDIFG. Two immunoreactive bands of approximately 140 kDa and 110 kDa were detected in adult amphioxus extracts

(Figure 3G). Band multiplicity could correspond to two protein isoforms generated by alternative splicing of NOS transcripts, as reported for mouse, human and *Drosophila* NOS [27, 28], or to proteolytic cleavage at the N-terminal domain [29]. Whole-mount immunostaining showed NOS expression also during amphioxus development. While no obvious staining other than background was observed at early developmental stages (data not shown), *B. floridae* 48 h larvae showed a strong signal confined to the mid- and hindgut of the developing intestine and the dorsal region of the club-shaped gland (csg), an enigmatic secretory organ located on the right side of the larval pharynx between the endostyle and the anterior-most pharyngeal gill slit (Figure 3, A and B). In the first, the NOS signal was separated by a non-stained segment, which corresponds to the ilio-colon ring, an specialized region with conspicuous cilia that contributes to the food cord passage. Confocal sections revealed a left-right NOS asymmetry in the midgut area (Figure 3, C-E), with a triangular region at the left side devoid of signal that corresponds to the lateral ciliated tract. Concerning cgs expression, although the dorsal and ventral cells are not morphologically different, the specific NOS expression to the dorsal area reveals functional differences along the dorsal-ventral axis, as reported for other amphioxus genes, e.g. *Krox* [30] and *crabp* [31] to the dorsal region, and *maf* [31] and *BbPtx* [32] to the ventral duct.

Figure 2. (A). Comparison of the deduced amino acid sequences of *B. floridae* NOS (Bf NOS) with human (Hs nNOS, iNOS and eNOS) and *Drosophila* (Dm NOS) forms. Strictly conserved and highly conserved residues (>60%) are shown in black background, and similar residues in gray. Defined binding domains (as in [27]) are overlined in red: cofactor-binding sites for heme (1), calmodulin (2), FMN (3), FAD pyrophosphate (4), FAD isoalloxazine (5), NADPH ribose (6), NADPH adenine (7) and the C-terminal conserved NADPH binding sequence (8). The sequence used for phylogenetic analyses begins at position D352 of human nNOS (*). (B) Phylogenetic reconstruction of NOS enzymes. Figures at nodes are the scores from 1000-bootstraps resampling of the data (NJ, in black) or quartet puzzling supports values (ML, in red). Ac, *Aplysia californica*, California sea hare; As, *Anopheles stephensi*; Bm, *Bombyx mori*; Cc, *Cyprinus carpio*, carp; Dr, *Danio rerio*, zebrafish; Dm, *Drosophila melanogaster*; Gg, *Gallus gallus*; Hs, *Homo sapiens*; Ls, *Lymnaea stagnalis*, great pond snail; Ms, *Manduca sexta*, tobacco hornworm; Mm, *Mus musculus*; Om, *Oncorhynchus mykiss*, rainbow trout; Rr, *Rattus norvergicus*; Rp, *Rhodnius prolixus*, insect; Sp, *Strongylocentrotus purpuratus*, sea urchin; Tp, *Takifugu poecilonotus*; Xt, *Xenopus tropicalis*.

A)

		Length
Hs-nNOS	MEDHMFGVQQIQPNVISVRLFKRKVGGGLFLVKERVS KPPVIISDLIRGGAAEQLGIIAGDIIIAVNNGRPTEVDLSDYSALEVLRGIASETHVVLILRGPETFTTLETTFTTDGTPKTI	120
Hs-eNOS		
Bf-nNOS		
Dm-nNOS	-MSQHFTSIFENLRFVTIKRATN-----	
Hs-nNOS	RVTQPLGPPTKAVDLSHOPPAKEQPLAVIDGASGPNGPQHAYDDQEAQSLEPHANGLA PRPGQDPARKTRVSLQGRGENNEELKIEPVPLSLLTS	240
Hs-eNOS	-M4CP-----	28
Bf-nNOS	-M6NLSKSWAO3D-----	21
Dm-nNOS	-AQQQQQQQQQQQQQQQQQQKQAKTQQQNNSRKIK-----	46
Hs-nNOS	-TQATPTLNNGL-----	70
Hs-nNOS	DRDLGCKSHKPLLGIVENDRVFDLWKGKNNVPPVNLNPYSEKECPMSGKSPTKNSPSKCPFLKVKNWETEVVDTLHLKSTLTETCCKEYICWGSIMFQSQHARPE-DVTKGQH	359
Hs-eNOS	EXAPQGCGG-TTODDLOVNLKQONESQ-----	139
Hs-eNOS	-EPCGKSPSVELVLDL-----	123
Bf-nNOS	-ADPASL-----	133
Dm-nNOS	-LEGNPNQGGDSSPSHEVDPGG-----	268
Hs-nNOS	DRDLGCKSHKPLLGIVENDRVFDLWKGKNNVPPVNLNPYSEKECPMSGKSPTKNSPSKCPFLKVKNWETEVVDTLHLKSTLTETCCKEYICWGSIMFQSQHARPE-DVTKGQH	359
Hs-eNOS	EXAPQGCGG-TTODDLOVNLKQONESQ-----	139
Hs-eNOS	-EPCGKSPSVELVLDL-----	123
Bf-nNOS	-RGNTTDEKARLIRELENNGDIFLY-ERGVANGDVIXSINGCTIANCPCVICHRS-----	248
Dm-nNOS	-QW&CFFP-SQASGKSS-----	268
Hs-nNOS	DRDLGCKSHKPLLGIVENDRVFDLWKGKNNVPPVNLNPYSEKECPMSGKSPTKNSPSKCPFLKVKNWETEVVDTLHLKSTLTETCCKEYICWGSIMFQSQHARPE-DVTKGQH	359
Hs-eNOS	FPLAKEFPIQYSSSIRFKPSKANMEREEKQKIDDTSTKQKETDLYIYAKHAWRNARCSVGRIQWSKLQVF DARDCTAAGMNYICNHVKYATNCNLRSAITFPQRTDGKHDPRV	479
Hs-eNOS	LPQIAIEFVNQYYGSPREAKIEELA-----	259
Hs-eNOS	-PRAPEHSPSPSPLT-----	243
Bf-nNOS	-LEQAEKFIFPEYASL-----	368
Dm-nNOS	-LEHAKDFLEQYITSIKRTSCT-----	388
Hs-nNOS	WNSQIPIRYAGQDGSITGDPANVQFTCIGQGWKPPGRPDVPLFLQANGNDPELCPPEPLVLEVDTFRPKTFWKLGPAPSNMLL-----	599
Hs-eNOS	WNAQIPIRYAGQDGSITGDPANVQFTCIGQGWKPPGRPDVPLFLQANGNDPELCPPEPLVLEVDTFRPKTFWKLGPAPSNMLL-----	363
Bf-nNOS	WNQGPFLKYMAYQDGSV-----	488
Dm-nNOS	WNWNLQISIYAGYQDAGKINGDPMVFEWV-----	508
Hs-nNOS	VRDYCDNSRNYNILEVAKEMNLMRKTSSLWKSQALQEINIAVLYSFQSDKVTIVDHSAESFJHKMENEYRCKGGP PADWVWIVPPMSGSIPTVPHQEM-NYRLTPSFYQDPDWNT	719
Hs-eNOS	TNLMLGTVRYNILEVGRMLGTLTHL-----	499
Bf-nNOS	TRDLCDAERLNTEAVGKRMGLVARNSLWLKD-----	607
Dm-nNOS	SMLNCDTTRRNLETVALMQLDTRPTSLWKS-----	628
Hs-nNOS	WVWKG-----	829
Hs-eNOS	WVQD-----	608
Hs-eNOS	-TGITTRK-----	589
Bf-nNOS	WRKKPKHPVLLKFAYDENPRCS-----	726
Dm-nNOS	WVKKGRGE-----	741
Hs-nNOS	LEMHRHPNSVQ-----	932
Hs-eNOS	LPML-----	669
Hs-eNOS	LEMMSGVPRYNS-----	695
Bf-nNOS	LHMHPHPGSD-----	825
Dm-nNOS	LYAMIVQESSEHGLQDSSSTGSSKSMKA-----	861
Hs-nNOS	RWAKKVFKAACDVFQCVGCDVNIEKINN-----	1048
Hs-eNOS	RWAVQTFKRACTE-----	809
Bf-nNOS	RWQAQAFKFACTEDVGDVNME-----	943
Dm-nNOS	RWAEVFKFLACETCFEDPEEISLSDA-----	974
Hs-nNOS	VIALLERELDAEPVNOMWVKEVLEDEERNTALGVISNWTDELRLP-----	1168
Hs-eNOS	VQG-----	896
Bf-nNOS	VBALLSRUEPDPAPTEPVAVE-----	928
Dm-nNOS	WDGLINRZGVDNPDEVLOLO-----	1063
Hs-nNOS	WQAKLJLOPRYYSISSSPDRVSDEIHLTVA-----	1283
Hs-eNOS	WQYEAQKAVAVQPS-----	1011
Hs-eNOS	WVFGCRCSOLDECTYV-----	1043
Bf-nNOS	WVFGCQSRDHTY-----	1181
Dm-nNOS	WQOLTLQFPRYSISSSPDRVSDEIHLTVA-----	1210
Hs-nNOS	WVFGCRQSKTIDILY-----	1403
Hs-eNOS	WVFGCR-----	1131
Hs-eNOS	WVFGCRCSOLDECTYV-----	1163
Bf-nNOS	WVFGCQSRDHTY-----	1301
Dm-nNOS	WPFGRNRDVT-----	1328
Hs-nNOS	WVFGCRQSKTIDILY-----	1434
Hs-eNOS	WVFGCR-----	1153
Hs-eNOS	WVFGCRCSOLDECTYV-----	1203
Bf-nNOS	WVFGCQSRDHTY-----	1329
Dm-nNOS	WTAIHIKTSRATARERMASQP-----	1350

B)

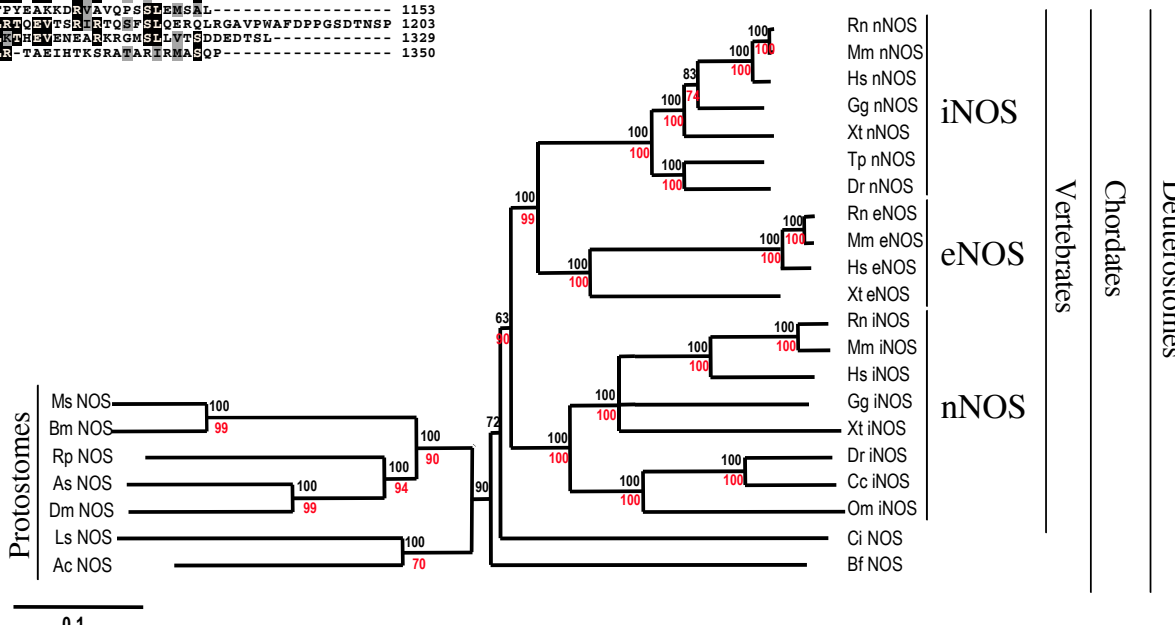


Figure 3. Whole-mount immunostaining of 48 h *B. floridae* larvae with an anti-NOS antibody. (A) Right-sided view. NOS signalling in the developing midgut and hindgut region separated by a non stained area, the ilio-colon ring (arrow), and in the dorsal region of the club-shaped gland (arrowhead). (B) Left-sided view. NOS signalling in the gut shows two non stained regions, which correspond to the ilio-colon ring (arrow) and to the lateral ciliated tract (double arrowhead). (C-E) Magnified view of the confocal sections of the right side, light and left side of the gut, respectively, showing left-right asymmetry in NOS localization. (F) Detail of the NOS staining in the dorsal region of the club-shaped gland (arrowhead). (G) Western blot analysis of amphioxus protein extracts. A total of 1.0 mg of soluble protein extract were resolved by electrophoresis on a SDS-7.5% polyacryla-mide gel, transferred to a polyvinylidene difluoride (PVDF) membrane and incubated with an anti-NOS antibody. Positions of molecular mass markers (in kDa) are shown on the left. (H) *Adh3* expression visualized by whole-mount *in situ* hybridization as reported in [17].



4. Discussion

The housekeeping role long attributed to ADH3 as a formaldehyde detoxifying enzyme has been lately challenged after *in situ* analyses and studies on the activity of the enzyme. Concerning expression, the tissue-specificity observed for ADH3 in amphioxus and other invertebrates [17, 18] was difficult to reconcile with the assumed general cytoprotective role for this enzyme. In relation to the biochemical activity, human and rat ADH3 used substrates other than formaldehyde, such as GSNO [12, 14, 26]. Moreover, we here show a GSNO_R activity for the recombinant *B. floridae* ADH3, 2-fold higher than for HMGSH (Table 1), and preservation of the ADH3 kinetic features during the invertebrate/vertebrate transition, when the ADH family expanded considerably through a series of duplications [25]. Based on the strict preservation of the protein structure and the biochemical activities, including those shown in the present study, we assume that the ancestral ADH3 was a multifunctional enzyme, active in HMGSH and GSNO metabolisms.

The biochemical data pointed to a functional role for the cephalochordate ADH3 in the NO

homeostasis. To link the ADH3 gut-restricted expression with the NO/GSNO production, we aimed at characterizing the amphioxus *Nos* genes. Surveys of *B. floridae* databases rendered a single-copy *Nos* that showed gut-specific expression in developing larvae. Phylogenetically, the amphioxus NOS protein branched outside the clade that comprised all the vertebrate forms, indicating that the *Nos* duplications took place after the cephalochordate divergence. The topology of the tree also suggested that *Nos* duplicated at least twice during vertebrate evolution: the nNOS enzymes aroused after the first duplicative event, while the iNOS and eNOS were generated after the second. The increase in complexity, probably concomitant with novel areas of NO production, could be linked to the almost generalized ADH3 expression observed in vertebrates [18, 33] and improved the regulation of NO/GSNO homeostasis.

In situ and immunostaining analyses in amphioxus revealed an almost full overlap of the ADH3 and NOS expression patterns and showed the larval intestine as the major organ for NO synthesis and degradation. In vertebrates, the *in vivo* contribution of ADH3 in NO metabolism was established in ADH3 knockout mice, whose major

functional alteration was an increase in intracellular SNO-protein levels under basal conditions [9, 11], effect that was greatly enhanced after endotoxic or bacterial challenge. During host defence responses, vertebrate iNOS is strongly induced [34, 35] and S-nitrosothiols are currently involved to respond to cryptococcal, salmonella and tuberculous infections [36-38]. NO is also involved in the molluscan [39] and *Drosophila* [40] defence systems that, in the latter, are thought to originate mainly in the fat body, where *Drosophila* ADH3 is also strongly expressed [18]. Overall, the overlapping signals of amphioxus ADH3 and NOS (compare panels A and B with H in Figure 3) could account for a GSNO anti-microbial activity in the gut, where the first host-pathogen interaction takes place, and it is therefore prone to bacterial infections.

Acknowledgements

The authors acknowledge the critical comments raised by the reviewers that have substantially improved the scope of the discussion section. This work was supported by Ministerio de Ciencia y Tecnología (Spain), grant BMC2003-05211. LG was awarded FPI fellowship from CIRIT (Generalitat de Catalunya).

Conflict of interest

The authors have declared that no conflict of interest exists.

References

1. Feelisch M, Martin JF. The early role of nitric oxide in evolution. *Trends Ecol Evol* 1995; 10:496-499.
2. Stamler JS, Lamas S, Fang FC. Nitrosylation, the prototypic redox-based signaling mechanism. *Cell* 2001; 106:675-683.
3. Colasanti M, Venturini G, Merante A, et al. Nitric oxide involvement in *Hydra vulgaris* very primitive olfactory-like system. *J Neurosci* 1997; 17:493-499.
4. Frogget SJ, Leise EM. Metamorphosis in the marine snail *Ilyanassa obsoleta*, Yes or NO? *Biol Bull* 1999; 196:57-62.
5. Giovine M, Pozzolini M, Favre A, et al. Heat stress-activated, calcium-dependent nitric oxide synthase in sponges. *Nitric Oxide* 2001; 5:427-431.
6. Koh HY, Jacklet JW. Nitric oxide induces cGMP immunoreactivity and modulates membrane conductance in identified central neurons of *Aplysia*. *Eur J Neurosci* 2001; 13:553-560.
7. Kim HW, Batista LA, Hoppes JL, et al. A crustacean nitric oxide synthase expressed in nerve ganglia, Y-organ, gill and gonad of the tropical land crab, *Gecarcinus lateralis*. *J Exp Biol* 2004; 207:2845-2857.
8. Regulski M, Stasiv Y, Tully T, et al. Essential function of nitric oxide synthase in *Drosophila*. *Curr Biol*. 2004; 14:R881-882.
9. Liu L, Yan Y, Zeng M, et al. Essential roles of S-nitrosothiols in vascular homeostasis and endotoxic shock. *Cell* 2004; 116:617-628.
10. Hess DT, Matsumoto A, Kim SO, et al. Protein S-nitrosylation: purview and parameters. *Nat Rev Mol Cell Biol* 2005; 6:150-166.
11. Liu L, Hausladen A, Zeng M, et al. A metabolic enzyme for S-nitrosothiols conserved from bacteria to humans. *Nature* 2001; 410:490-494.
12. Jensen DE, Belka GK, DuBois GC. S-Nitrosoglutathione is a substrate for rat alcohol dehydrogenase class III isoenzyme. *Biochem J* 1998; 2:659-668.
13. Sakamoto A, Ueda M, Morikawa H. *Arabidopsis* glutathione-dependent formaldehyde dehydrogenase is an S-nitrosoglutathione reductase. *FEBS Lett* 2002; 515:20-24.
14. Fernandez MR, Biosca JA, Pares X. S-nitrosoglutathione reductase activity of human and yeast glutathione-dependent formaldehyde dehydrogenase and its nuclear and cytoplasmic localisation. *Cell Mol Life Sci* 2003; 60:1013-1018.
15. Koivusalo M, Baumann M, Uotila L. Evidence for the identity of glutathione-dependent formaldehyde dehydrogenase and class III alcohol dehydrogenase. *FEBS Lett* 1989; 257:105-109.
16. González-Duarte R, Albalat R. Merging protein, gene and genomic data: the evolution of the MDR-ADH family. *Heredity* 2005; 95:184-197.
17. Cañestro C, Hjelmqvist L, Albalat R, et al. Amphioxus alcohol dehydrogenase is a class 3 form of single type and of structural conservation but with unique developmental expression. *Eur J Biochem* 2000; 267:6511-6518.
18. Cañestro C, Godoy L, González-Duarte R, et al. Comparative expression analysis of *Adh3* during arthropod, urochordate, cephalochordate and vertebrate development challenges its predicted housekeeping role. *Evol. Dev.* 2003; 5:157-162.
19. Uotila L, Koivusalo M. Multiple forms of formaldehyde dehydrogenase from human red blood cells. *Hum Hered* 1987; 37:102-106.
20. Thompson JD, Gibson TJ, Plewniak F, et al. The CLUSTAL_X windows interface: flexible strategies for multiple sequence alignment aided by quality analysis tools. *Nucleic Acids Res* 1997; 25:4876-4882.
21. Page RDM. TREEVIEW: An application to display phylogenetic trees on personal computers. *Comput. Appl. Biosci* 1996; 12:357-358.
22. Pollock VP, McGettigan J, Cabrero P, et al. Conservation of capa peptide-induced nitric oxide signalling in Diptera. *J Exp Biol.* 2004; 207:4135-4145.
23. Yasui K, Tabata S, Ueki T, et al. Early development of the peripheral nervous system in a lancelet species. *J Comp Neurol* 1998; 393:415-425.
24. Danielsson O, Atrian S, Luque T, et al. Fundamental molecular differences between alcohol dehydrogenase classes. *Proc Natl Acad Sci USA* 1994; 91:4980-4984.
25. Cañestro C, Albalat R, Hjelmqvist L, et al. Ascidian and Amphioxus Adh genes correlate functional and molecular features of the ADH Family expansion during vertebrate evolution. *J Mol Evol* 2002; 54:81-89.
26. Hedberg JJ, Griffiths WJ, Nilsson SJ, et al. Reduction of S-nitrosoglutathione by human alcohol dehydrogenase 3 is an irreversible reaction as analysed by electrospray mass spectrometry. *Eur J Biochem*. 2003; 270:1249-1256.
27. Regulski M, Tully T. Molecular and biochemical characterization of dNOS: a *Drosophila* Ca²⁺/calmodulin-dependent nitric oxide synthase. *Proc Natl Acad Sci USA* 1995; 92:9072-9076.
28. Ogura T, Yokoyama T, Fujisawa H, et al. Structural diversity of neuronal nitric oxide synthase mRNA in the nervous system. *Biochem Biophys Res Commun*. 1993; 193:1014-1022.
29. Sengupta R, Sahoo R, Mukherjee S, et al. Characterization of *Drosophila* nitric oxide synthase: a biochemical study. *Biochem Biophys Res Commun*. 2003; 306:590-597.
30. Knight RD, Panopoulou GD, Holland PW, et al. An amphioxus *Krox* gene: insights into vertebrate hindbrain evolution. *Dev Genes Evol* 2000; 210:518-521.
31. Jackman WR, Mougey JM, Panopoulou GD, et al. *crabp* and *maf* highlight the novelty of the amphioxus club-shaped glan. *Acta Zool* 2004; 85:91-99.
32. Yasui K, Zhang S, Uemura M, et al. Left-right asymmetric expression of *BbPtx*, a *Ptx*-related gene, in a lancelet species and

- the developmental left-sidedness in deuterostomes. *Development* 2000; 127:187-195.
33. Ang HL, Deltour L, Hayamizu TF, et al. Retinoic acid synthesis in mouse embryos during gastrulation and craniofacial development linked to class IV alcohol dehydrogenase gene expression. *J Biol Chem* 1996; 271:9526-9534.
34. Laubach VE, Foley PL, Shockley KS, et al. Protective roles of nitric oxide and testosterone in endotoxemia: evidence from NOS-2-deficient mice. *Am J Physiol*. 1998; 275:H2211-2218.
35. Nicholson SC, Hahn RT, Grobmyer SR, et al. Echocardiographic and survival studies in mice undergoing endotoxic shock: effects of genetic ablation of inducible nitric oxide synthase and pharmacologic antagonism of platelet-activating factor. *J Surg Res*. 1999; 86:198-205.
36. De Groot MA, Testerman T, Xu Y, et al. Homocysteine antagonism of nitric oxide-related cytostasis in *Salmonella typhimurium*. *Science*. 1996; 272:414-417.
37. MacMicking JD, North RJ, LaCourse R, et al. Identification of nitric oxide synthase as a protective locus against tuberculosis. *Proc Natl Acad Sci USA*. 1997; 94:5243-5248.
38. de Jesus-Berrios M, Liu L, Nussbaum JC, et al. Enzymes that counteract nitrosative stress promote fungal virulence. *Curr Biol* 2003; 13:1963-1968.
39. Conte A, Ottaviani E. Nitric oxide synthase activity in molluscan hemocytes. *FEBS Lett*. 1995; 365:120-124.
40. Foley E, O'Farrell PH. Nitric oxide contributes to induction of innate immune responses to gram-negative bacteria in *Drosophila*. *Genes Dev*. 2003; 17:115-125.